Science Arts & Métiers (SAM)

is an open access repository that collects the work of Arts et Métiers Institute of Technology researchers and makes it freely available over the web where possible.

This is an author-deposited version published in: https://sam.ensam.eu
Handle ID: .http://hdl.handle.net/10985/26026

To cite this version :

Francisco J. VALDÉS-PARADA, Didier LASSEUX - Clarifications about upscaling diffusion with heterogeneous reaction in porous media - Acta Mechanica - 2025

Any correspondence concerning this service should be sent to the repository Administrator : scienceouverte@ensam.eu

Arts et Métiers Institute of Technology

Acta Mech
https://doi.org/10.1007/s00707-024-04214-4

ORIGINAL PAPER

Francisco J. Valdés-Parada · Didier Lasseux

Clarifications about upscaling diffusion with heterogeneous reaction in porous media

Received: 11 April 2024 / Revised: 22 December 2024 / Accepted: 27 December 2024
© The Author(s), under exclusive licence to Springer-Verlag GmbH Austria, part of Springer Nature 2025

Abstract The upscaling process of coupled (single- and two-species) diffusion with heterogeneous chemical reaction in homogeneous porous media is revisited in this work with several important clarifications following the article from Bourbatache et al. (Acta Mech 234: 2293-2314, 2023. https://doi.org/10.1007/s00707-023-03501-w). It is shown that the upscaled model obtained from the volume averaging method (VAM) or, equivalently, following an adjoint and Green's formulation technique provides a closed model without any *a priori* assumption on the form of the solution for the pore-scale concentration involved in the spectral approach used in the periodic homogenization method (PHM) reported in the above reference. Through comparison with direct pore-scale simulations, the VAM model is shown to outperform the predictions of the average concentration and average flux profiles for the simple two-dimensional configuration considered in Bourbatache et al. (Acta Mech 234: 2293-2314, 2023. https://doi.org/10.1007/s00707-023-03501-w) in comparison with the model obtained from PHM in this reference. Finally, identification of the apparent effective diffusion coefficient from these pore-scale simulations, which serve as *in silico* experiments, proves that the correct dependence upon the Damkhöler number is the one predicted by the model obtained with VAM, in contradiction with the conclusion put forth in Bourbatache et al. (Acta Mech 234: 2293-2314, 2023. https://doi.org/10.1007/s00707-023-03501-w). The physical explanation lies in the corrective contribution of the reactive part to the apparent effective diffusion coefficient, which is positive and adds up to the pure intrinsic diffusive part. The discrepancy between PHM and VAM approaches is proved to originate from the choice of changes of variables in the pore-scale concentration used in the spectral approach while employing PHM.

1 Introduction

Modeling coupled chemical species mass diffusion and reaction processes in homogeneous porous media at the macroscopic scale is of major importance for many applications including chemical engineering processes (cf. [1–3]), microporous electrodes [4–8], underground mechanisms encountered in hydrology (cf. [9–11]) and materials manufacturing, like composites (cf. [12]), biological systems [13] and many others. Efforts have

Francisco J. Valdés-Parada
Departamento de ingeniería de procesos e hidráulica, Universidad Autónoma Metropolitana-Iztapalapa, Av. San Rafael Atlixco 186, col. Vicentina, 09340 Mexico City, CDMX, Mexico
E-mail: iqfv@xanum.uam.mx

Didier Lasseux
I2M, UMR 5295, Univ. Bordeaux, CNRS, Bordeaux INP, 351, Cours de la Libération, CEDEX 33405 Talence, France

Didier Lasseux (✉)
I2M, UMR 5295, Arts et Metiers Institute of Technology, CNRS, Bordeaux INP, 351, Cours de la Libération, CEDEX 33405 Talence, France
E-mail: didier.lasseux@cnrs.fr

Published online: 30 January 2025

been dedicated to the derivation of macroscopic models obtained from the physical description at the pore scale and have been extensively reported in the literature (e.g., [2,9,14]).

Regardless the upscaling approach, in particular using either the volume averaging method (VAM) [15–20] or the periodic homogenization method (PHM) [21–24], the derived macroscopic models are in perfect agreement in the regime for which the characteristic time of reaction, t^r_{ref}, remains larger than or equal to that of diffusion, t^d_{ref}, at the pore scale, i.e., when the Damköhler number, $Da = \frac{t^d_{ref}}{t^r_{ref}} \leq 1$. However, the regime corresponding to $Da > 1$ was recently reconsidered by Bourbatache et al. [21] in which a macroscopic model using PHM previously derived in [24] was compared to that obtained from VAM [20]. Many significant differences between the two macroscopic models were highlighted in [21], and this raises several questions that trigger the analysis reported in the present work. Indeed, although the overall mathematical structure of the macroscopic models obtained from both approaches is the same, the effective coefficients appearing in them are different as they are obtained from clearly different closure problems. Illustrations of the contrasting predictions of the effective diffusion coefficient are reported in Fig. 5 in [21], considering a coupled diffusion–reaction process of two chemical species in the transverse direction of a simple structure made of a square pattern of parallel cylinders of circular cross section. More specifically, it was observed that (i) the normalized effective reaction rates obtained from PHM and VAM differ in values but have the same trend of dependence on Da, (ii) the so-called effective diffusion coefficients from these two methods differ both in values and dependence upon Da. Indeed, the effective diffusion coefficient obtained from VAM (respectively, PHM) is an increasing (respectively, decreasing) function of Da. Nevertheless, the predictions of the steady macroscopic (average) concentration and diffusive flux of the diffusing/reacting species seem to perform equally well, as reported in Figs. 9 and 10 in [21]. This obviously raises the question about which approach predicts the correct dependence of the diffusion coefficient on Da.

The purpose of this work is to cautiously inspect the models obtained from VAM and PHM in the range of $Da \geq 1$ in order to clearly address the above-mentioned controversy. To this aim, the main steps of the VAM leading to the macroscopic model and associated closure problems that provide the effective coefficients are recalled in Sect. 2.1.1. It is further shown that the same macroscale model and closure problems are obtained employing the adjoint and Green's formulation approach that is detailed in Appendix A. The model contains effective diffusion and reaction terms, but it also involves a convective-like term arising from the upscaling process. This term is usually neglected on the basis of orders of magnitude estimates [cf. [2], Chap.1]. In Appendix B, it is shown, by means of Green's formula, that this term is indeed equal to zero. In Appendix C, the effective diffusion tensor is shown to be symmetric and positive. Moreover, a decomposition of the closure problem yielding the effective diffusion tensor is provided that allows one to separately identify the pure diffusive contribution, which is intrinsic and constant for a given structure, and the contribution from reaction that is function of both the pore structure and Da. Next, the model obtained with PHM, as reported by Bourbatache et al. [21,24], together with the corresponding ancillary problems from which the effective coefficients are obtained, are summarized in Sect. 2.1.2. The methodology employed in these references follows the works of Mauri [22] and Allaire and Raphael [23] in which a difficulty encountered in the homogenization method has been alleviated by assuming an *a priori* form of the pore-scale concentration dependence upon time and space that leads to a spectral approach. The consequences of these assumptions, frequently used by some authors, have not been discussed in detail in the literature. In Appendix D, it is shown that the discrepancy in the effective coefficients obtained from PHM and VAM lies in the change of variable in the pore-scale concentration employed in the spectral approach with PHM, and not in the upscaling methods themselves. The extension of the macroscopic model to the case of two diffusing-reacting species, as envisaged in [21], is shortly addressed in Sect. 2.2. Section 3 is dedicated to the analysis, comparison and validation of the macroscale model by means of numerical simulations. In particular, it is shown that the data reported in [21] are in error regarding VAM for both the effective diffusion coefficient and the effective reaction rate in the case of one species, as well as for the effective co-diffusion coefficient in the case of two species, (cf. Fig. 5 in this reference). Moreover, a comparison of the predictions obtained from the analytical solutions of the VAM and PHM macroscopic models with pore-scale simulation results is presented in terms of the average concentration and diffusive flux. The comparison shows that the VAM model outperforms with respect to the PHM model reported by Bourbatache et al. [21]. In addition, the conclusion put forth by the authors of the latter reference, which states "*Nevertheless, the PHM results seem to be more coherent from a physical point of view. Indeed, the chemical reactions at the solid–fluid interface must slow down the diffusive transfer, leading to a decreasing of the homogenized diffusion tensors*," is shown to be in error. In fact, direct pore-scale simulations, which correspond to *in silico* experiments, demonstrate that the effective diffusion coefficient (which should

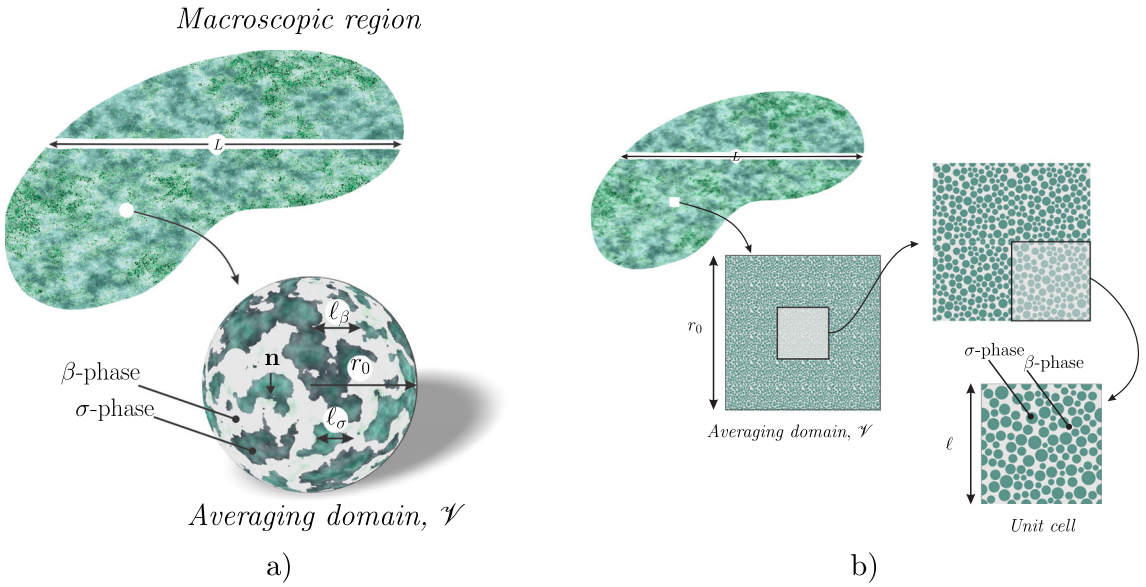

Fig. 1 Sketch of a porous medium system highlighting: **a** the averaging domain, the phases and the main characteristic lengths and **b** a representation of the medium using periodic unit cells

be better called apparent effective diffusion coefficient) increases with Da and that the computed values are in very good agreement with the predictions obtained from VAM, definitely validating this model and solving the controversy that motivated this work. The physical explanation lies in the fact that the apparent effective diffusion coefficient contains a corrective contribution from reaction, which increases with Da and adds up to the pure diffusive effect. Conclusions are finally drawn in Sect. 4.

2 Recall on upscaled models

2.1 One-species diffusion and heterogeneous reaction

This section focuses on the case where only one diluted species, of molar concentration c in the fluid phase, *i.e.*, the β phase, is diffusing and experiencing a heterogeneous reaction at the solid–fluid interface, $\mathscr{A}_{\beta\sigma}$, the σ phase denoting the solid phase (see Fig. 1a). The corresponding pore-scale problem is given by [2]

$$\frac{\partial c}{\partial t} = \nabla \cdot (\mathscr{D} \nabla c)\,, \quad \text{in } \mathscr{V}_\beta, \tag{1a}$$

$$B.C. \quad -\mathbf{n} \cdot \mathscr{D} \nabla c = kc, \quad \text{at } \mathscr{A}_{\beta\sigma}. \tag{1b}$$

Here, $\mathscr{D}$ is the molecular diffusion coefficient; k is the reaction rate for the first-order kinetics of the heterogeneous reaction. Moreover, $\mathscr{V}_\beta$ (of volume V_β) represents the domain occupied by the β phase inside the averaging domain, $\mathscr{V}$ (of size r_0 and volume V, see Fig. 1a)), so that the intrinsic average concentration $\langle c \rangle^\beta$ is defined as

$$\langle c \rangle^\beta = \frac{1}{V_\beta} \int_{\mathscr{V}_\beta} c \, dV. \tag{2}$$

Macroscopic boundary conditions and an initial condition, which should also be specified for completeness of the above problem statement, are omitted since they are not used in the developments of the upscaled models.

2.1.1 Volume averaging method (VAM)

To obtain the macroscopic model using the volume averaging method (VAM), c is decomposed into its intrinsic average and spatial deviation, $\tilde{c}$, according to [25]

$$c = \langle c \rangle^{\beta} + \tilde{c}. \tag{3}$$

Following the developments reported in [2,17,19], the unclosed macroscopic model can be written as

$$\frac{\partial \langle c \rangle^{\beta}}{\partial t} = \nabla \cdot \left[\mathscr{D} \left(\nabla \langle c \rangle^{\beta} + \frac{1}{V_{\beta}} \int\limits_{\mathscr{A}_{\beta\sigma}} \mathbf{n} \tilde{c} \, dA \right) \right] - \frac{k a_v}{\phi} \langle c \rangle^{\beta} - \frac{k}{V_{\beta}} \int\limits_{\mathscr{A}_{\beta\sigma}} \tilde{c} \, dA. \tag{4}$$

In this expression, $\mathbf{n}$ is the unit normal vector at $\mathscr{A}_{\beta\sigma}$, pointing out of the β phase (see Fig. 1a), a_v is the interfacial area per unit volume of the porous medium ($a_v \equiv A_{\beta\sigma}/V$, $A_{\beta\sigma}$ being the area of $\mathscr{A}_{\beta\sigma}$), whereas ϕ is the porosity of the medium. To arrive at this result, length scales separation was assumed, i.e., $\ell_{\beta} \ll r_0 \ll L$, where ℓ_{β} represents the characteristic pore size and L the macroscopic size of interest, for instance, the size of the system. In these developments, the averaging domain, $\mathscr{V}$, is assumed to be representative so that average quantities can be treated as constants within it. In addition, the porous medium is assumed to be spatially homogeneous, so that $\nabla \phi = \mathbf{0}$. Equation (4) is yet unclosed, since both the average concentration $\langle c \rangle^{\beta}$ and concentration deviation $\tilde{c}$ are involved.

A closed macroscopic model can be derived by formally using an adjoint and Green's formulation methodology [26], as detailed in Appendix A. This methodology leads to the same average model and associated closure (adjoint) problems as those obtained with the classical volume averaging method summarized below. Following the latter approach, Eq. (4) is subtracted from the original pore-scale mass balance Eq. (1a) and, considering that $\mathscr{V}$ identifies with a representative periodic unit cell (see Fig. 1b) so that $\tilde{c}$ is periodic, the boundary value problem for $\tilde{c}$ can be written as follows [17,19]

$$0 = \mathscr{D} \nabla^2 \tilde{c} + \frac{k a_v}{\phi} \langle c \rangle^{\beta} + \frac{k}{V_{\beta}} \int\limits_{\mathscr{A}_{\beta\sigma}} \tilde{c} \, dA, \quad \text{in } \mathscr{V}_{\beta}, \tag{5a}$$

$$B.C. \quad -\mathbf{n} \cdot \mathscr{D} \nabla \tilde{c} - k \tilde{c} = \mathbf{n} \cdot \mathscr{D} \nabla \langle c \rangle^{\beta} + k \langle c \rangle^{\beta}, \quad \text{at } \mathscr{A}_{\beta\sigma}, \tag{5b}$$

$$\tilde{c}(\mathbf{r}) = \tilde{c}(\mathbf{r} + \mathbf{l}_i), \quad i = 1, 2, 3, \tag{5c}$$

$$\langle \tilde{c} \rangle^{\beta} = 0. \tag{5d}$$

While writing Eq. (5a), it is assumed that the characteristic time t^* at which the process is observed in the unit cell is much larger than the characteristic time of diffusion at the pore scale, i.e., $t^* \gg \ell_{\beta}^2/\mathscr{D}$, so that $\tilde{c}$ can be assumed quasi-steady. In addition, on the basis of the periodicity assumption for both the geometry and $\tilde{c}$, the term $\frac{1}{V_{\beta}} \int_{\mathscr{A}_{\beta\sigma}} \mathbf{n} \tilde{c} \, dA$, is regarded as a constant, so that its spatial variations are zero. In Eq. (5c), $\mathbf{l}_i$ denotes the periodic lattice vector in the ith direction. Moreover, the average constraint expressed in Eq. (5d) follows from the application of the intrinsic volume averaging operator defined in Eq. (2) to the decomposition of c expressed in Eq. (3) and the separation of length scales assumption.

The boundary value problem for $\tilde{c}$ expressed in Eq. (5) is linear and made nonhomogeneous by the macroscopic sources involving $\langle c \rangle^{\beta}$ and $\nabla \langle c \rangle^{\beta}$ present in Eqs. (5a) and (5b). Therefore, the formal solution for $\tilde{c}$ can be expressed by means of a linear combination of these sources, namely

$$\tilde{c} = \mathbf{d} \cdot \nabla \langle c \rangle^{\beta} + (s - 1) \langle c \rangle^{\beta}. \tag{6}$$

In this expression, the vector $\mathbf{d}$ and scalar s are closure variables that, respectively, map the influence of the sources, $\nabla \langle c \rangle^{\beta}$ and $\langle c \rangle^{\beta}$, onto $\tilde{c}$. Substituting this formal solution into Eq. (5), and separating the contribution from each macroscopic source, allows one to write the following two closure problems [17,19]

Problem I

$$\mathbf{0} = \mathscr{D}\nabla^2\mathbf{d} + \frac{k}{V_\beta}\int\limits_{\mathscr{A}_{\beta\sigma}} \mathbf{d}\, dA, \quad \text{in } \mathscr{V}_\beta, \tag{7a}$$

$$B.C. \quad -\mathbf{n}\cdot\mathscr{D}\nabla\mathbf{d} - k\mathbf{d} = \mathscr{D}\mathbf{n}, \quad \text{at } \mathscr{A}_{\beta\sigma}, \tag{7b}$$

$$\mathbf{d}(\mathbf{r}) = \mathbf{d}(\mathbf{r}+\mathbf{l}_i), \quad i = 1,2,3, \tag{7c}$$

$$\langle\mathbf{d}\rangle^\beta = \mathbf{0}. \tag{7d}$$

Problem II

$$0 = \nabla^2 f + \frac{k}{\mathscr{D}}, \quad \text{in } \mathscr{V}_\beta, \tag{8a}$$

$$B.C. \quad -\mathbf{n}\cdot\mathscr{D}\nabla f = kf, \quad \text{at } \mathscr{A}_{\beta\sigma}, \tag{8b}$$

$$f(\mathbf{r}) = f(\mathbf{r}+\mathbf{l}_i), \quad i = 1,2,3. \tag{8c}$$

In the latter problem, f is defined by the change of variable given by

$$f = \frac{\phi s}{a_v\langle s\rangle_{\beta\sigma}}, \tag{8d}$$

where $\langle s\rangle_{\beta\sigma} = \frac{1}{A_{\beta\sigma}}\int\limits_{\mathscr{A}_{\beta\sigma}} s\, dA$. Note that applying the intrinsic averaging operator to Eq. (6) and taking into account Eq. (7d) imply that s and f satisfy the following constraints

$$\langle s\rangle^\beta = 1, \quad \langle f\rangle^\beta = \frac{\phi}{a_v\langle s\rangle_{\beta\sigma}}. \tag{8e}$$

so that $s = f/\langle f\rangle^\beta$. The formal solution given in Eq. (6) can now be substituted back into unclosed mass balance Eq. (4), yielding the closed macroscopic model, which can be written as

$$\frac{\partial\langle c\rangle^\beta}{\partial t} = \nabla\cdot\left(\mathbf{D}_{effr}\cdot\nabla\langle c\rangle^\beta\right) - \frac{a_v k_{eff}}{\phi}\langle c\rangle^\beta + \mathbf{u}\cdot\nabla\langle c\rangle^\beta. \tag{9}$$

In this model, the following nomenclature is adopted

$$\mathbf{D}_{effr} = \mathscr{D}\left(\mathbf{I} + \frac{1}{V_\beta}\int\limits_{\mathscr{A}_{\beta\sigma}} \mathbf{n}\mathbf{d}\, dA\right), \tag{10a}$$

$$a_v k_{eff} = \frac{\phi k}{\langle f\rangle^\beta}, \tag{10b}$$

$$\mathbf{u} = \frac{\mathscr{D}}{V_\beta\langle f\rangle^\beta}\int\limits_{\mathscr{A}_{\beta\sigma}} \mathbf{n} f\, dA - \frac{k}{V_\beta}\int\limits_{\mathscr{A}_{\beta\sigma}} \mathbf{d}\, dA, \tag{10c}$$

in which $\mathbf{D}_{effr}$ represents the apparent effective diffusion tensor, k_{eff} is the effective reaction rate coefficient and $\mathbf{u}$ is an effective velocity vector. However, as demonstrated in Appendix B, $\mathbf{u} = \mathbf{0}$, and the final macroscopic model obtained with VAM is given by

$$\phi\frac{\partial\langle c\rangle^\beta}{\partial t} = \nabla\cdot\left(\phi\mathbf{D}_{effr}\cdot\nabla\langle c\rangle^\beta\right) - a_v k_{eff}\langle c\rangle^\beta. \tag{11}$$

It must be emphasized that, in general, $\mathbf{D}_{effr}$ contains both diffusion and reaction effects. For this reason, it is preferable to use the terminology "apparent effective diffusion tensor" for this coefficient. The proof of symmetry and positiveness of $\mathbf{D}_{effr}$ is provided in Appendix C.

Under non-reactive conditions, macroscopic mass balance Eq. (11) reduces to

$$\phi \frac{\partial \langle c \rangle^{\beta}}{\partial t} = \nabla \cdot \left(\phi \boldsymbol{D}_{eff} \cdot \nabla \langle c \rangle^{\beta} \right). \tag{12}$$

Here, the effective diffusivity, $\mathbf{D}_{eff}$, is an intrinsic second-order tensor defined as [2]

$$\mathbf{D}_{eff} = \mathscr{D} \left(\mathbf{I} + \frac{1}{V_\beta} \int\limits_{\mathscr{A}_{\beta\sigma}} \mathbf{n}\mathbf{b}\, dA \right), \tag{13}$$

with $\mathbf{b} = \lim\limits_{k \to 0} \mathbf{d}$ solution of the following boundary value problem [2]

Problem I$\boldsymbol{b}$

$$\mathbf{0} = \nabla^2 \mathbf{b}\,, \quad \text{in } \mathscr{V}_\beta, \tag{14a}$$

$$B.C. \quad -\mathbf{n} \cdot \nabla \mathbf{b} = \mathbf{n}, \quad \text{at } \mathscr{A}_{\beta\sigma}, \tag{14b}$$

$$\mathbf{b}(\mathbf{r}) = \mathbf{b}(\mathbf{r} + \mathbf{l}_i), \quad i = 1, 2, 3, \tag{14c}$$

$$\langle \mathbf{b} \rangle^{\beta} = \mathbf{0}. \tag{14d}$$

It is worth mentioning that the intrinsic effective diffusivity tensor, $\mathbf{D}_{eff}$, can also be used under reactive conditions, as long as $Da \leq 1$ [19]. At this point, it is of interest to derive a relationship between the apparent effective diffusion tensor, $\mathbf{D}_{effr}$, and the intrinsic diffusion tensor, $\mathbf{D}_{eff}$. This can be achieved by proposing the following decomposition of closure variables

$$\mathbf{d} = \mathbf{b} + \mathbf{b}_r. \tag{15}$$

The new closure variable $\mathbf{b}_r$ solves the boundary value problem that results from subtracting Eq. (14) from Eq. (7) and writes

Problem I$\boldsymbol{b}_r$

$$-\frac{k}{V_\beta} \int\limits_{\mathscr{A}_{\beta\sigma}} \mathbf{b}\, dA = \mathscr{D} \nabla^2 \mathbf{b}_r + \frac{k}{V_\beta} \int\limits_{\mathscr{A}_{\beta\sigma}} \mathbf{b}_r\, dA, \quad \text{in } \mathscr{V}_\beta, \tag{16a}$$

$$B.C. \quad -\mathbf{n} \cdot \mathscr{D} \nabla \mathbf{b}_r - k\mathbf{b}_r = k\mathbf{b}, \quad \text{at } \mathscr{A}_{\beta\sigma}, \tag{16b}$$

$$\mathbf{b}_r(\mathbf{r}) = \mathbf{b}_r(\mathbf{r} + \mathbf{l}_i), \quad i = 1, 2, 3, \tag{16c}$$

$$\langle \mathbf{b}_r \rangle^{\beta} = \mathbf{0}. \tag{16d}$$

Furthermore, substituting the decomposition given in Eq. (15) into Eq. (10a), while recalling the definition of $\mathbf{D}_{eff}$ given in Eq. (13), leads to

$$\mathbf{D}_{effr} = \mathbf{D}_{eff} + \mathbf{D}_r. \tag{17}$$

Here, $\mathbf{D}_r$ is a correction to the intrinsic effective diffusion tensor due to reaction that is defined as

$$\mathbf{D}_r = \frac{\mathscr{D}}{V_\beta} \int\limits_{\mathscr{A}_{\beta\sigma}} \mathbf{n}\mathbf{b}_r\, dA. \tag{18}$$

Certainly, since $\mathbf{b}_r = \mathbf{0}$ under non-reactive conditions, it follows that $\mathbf{D}_r \to \mathbf{0}$ as $Da \to 0$. This trend is verified by numerical simulations of $\mathbf{D}_{effr}$ and $\mathbf{D}_r$ in Sect. 3.

2.1.2 Summary of the model derived by Bourbatache et al.

The mathematical structure of the upscaled model given in Eq. (11) corresponds to *case 3* referred to as "*Coupled diffusion–reaction model*" in [24] (for two chemical species), or as "*predominant reaction*" in [21] (for a single chemical species), which is the result of using the homogenization method involving a spectral approach (see also Eq. (D19)). However, the definitions of the effective medium coefficients in these works do not correspond to those reported in the previous section. For the sake of simplicity in notation, the superscript * used in [21] and [24] for dimensional quantities is dropped when referring to them in the rest of the present analysis. According to Bourbatache et al., the following dimensional definitions of the effective coefficients, $\boldsymbol{D}_r^{hom}$ and $\mathcal{K}$, should be used instead of $\mathbf{D}_{effr}$ and k_{eff}

$$\phi \mathbf{D}_{effr} \rightarrow \mathbf{D}_r^{hom} = \frac{1}{V} \int_{\mathscr{V}_\beta} \mathscr{D} \psi^2 (\mathbf{I} + \nabla_{\mathbf{y}} \boldsymbol{\chi}_r) \, dA = \phi \langle \mathscr{D} \psi^2 (\mathbf{I} + \nabla_{\mathbf{y}} \boldsymbol{\chi}_r) \rangle^\beta, \tag{19a}$$

$$a_v k_{eff} \rightarrow \mathcal{K} = \phi \lambda = \frac{a_v k}{\langle \psi \rangle^\beta} \left(\frac{1}{A_{\beta\sigma}} \int_{\mathscr{A}_{\beta\sigma}} \psi \, dA \right). \tag{19b}$$

Here, λ is the first eigenvalue, solution of the following closure problem
Problem ψ

$$-\nabla_{\mathbf{y}} \cdot \left(\mathscr{D} \nabla_{\mathbf{y}} \psi \right) = \lambda \psi, \quad \text{in } \mathscr{V}_\beta, \tag{20a}$$

$$B.C. \quad -\mathbf{n} \cdot \mathscr{D} \nabla_{\mathbf{y}} \psi = k \psi, \quad \text{at } \mathscr{A}_{\beta\sigma}, \tag{20b}$$

$$\psi(\mathbf{r}) = \psi(\mathbf{r} + \mathbf{l}_i), \quad i = 1, 2, 3, \tag{20c}$$

$$\langle \psi^2 \rangle^\beta = 1. \tag{20d}$$

Note that the expression of λ is extracted from Eq. (19b) and substituted in Eq. (20a) in order to obtain a problem on ψ only. Once this problem is solved, the field of ψ should be substituted into the following closure problem for $\boldsymbol{\chi}_r$
Problem $\boldsymbol{\chi}_r$

$$-\nabla_{\mathbf{y}} \cdot \left(\mathscr{D} \psi^2 (\mathbf{I} + \nabla_{\mathbf{y}} \boldsymbol{\chi}_r) \right) = \mathbf{0}, \quad \text{in } \mathscr{V}_\beta, \tag{21a}$$

$$B.C. \quad -\mathbf{n} \cdot \mathscr{D} \psi^2 (\mathbf{I} + \nabla_{\mathbf{y}} \boldsymbol{\chi}_r) = \mathbf{0}, \quad \text{at } \mathscr{A}_{\beta\sigma}, \tag{21b}$$

$$\boldsymbol{\chi}_r(\mathbf{r}) = \boldsymbol{\chi}_r(\mathbf{r} + \mathbf{l}_i), \quad i = 1, 2, 3, \tag{21c}$$

$$\langle \boldsymbol{\chi}_r \rangle^\beta = \mathbf{0}. \tag{21d}$$

In this way, all the information required for the prediction of the effective medium coefficients becomes available. However, it should be noted that identification of the pure diffusive part and corrective contribution of reaction seems out of reach in $\mathbf{D}_r^{hom}$ expressed in Eq. (19a).

Unfortunately, as reported in [21], $\mathbf{D}_r^{hom}$ differs from the effective diffusion tensor $\mathbf{D}_{effr}$ obtained from VAM given in Eq. (10a). It is therefore of interest to carefully analyze the similarities and differences of both approaches by means of numerical simulations. However, before proceeding with this, it is pertinent to show that the upscaled model derived above using VAM can also be used to study two-species diffusion and heterogeneous reaction in porous media.

2.2 Two-species diffusion and heterogeneous reaction

Recently, Bourbatache et al. [21] considered the process of two-species (A, B) diffusion and reversible heterogeneous reaction in homogeneous porous media. Assuming that the molecular diffusion coefficients are

constant and the same for both chemical species, the governing pore-scale equations and interfacial boundary conditions are given by

$$\frac{\partial c_A}{\partial t} = \mathscr{D}\nabla^2 c_A, \quad \text{in } \mathscr{V}_\beta, \tag{22a}$$

$$\frac{\partial c_B}{\partial t} = \mathscr{D}\nabla^2 c_B, \quad \text{in } \mathscr{V}_\beta, \tag{22b}$$

$$B.C.1 \quad -\mathbf{n}\cdot\mathscr{D}\nabla c_A = k_A c_A - k_B c_B, \quad \text{at } \mathscr{A}_{\beta\sigma}, \tag{22c}$$

$$B.C.2 \quad -\mathbf{n}\cdot\mathscr{D}\nabla c_B = -\left(k_A c_A - k_B c_B\right), \quad \text{at } \mathscr{A}_{\beta\sigma}. \tag{22d}$$

To decouple these problems, Bourbatache et al. [21] proposed the following changes of variables

$$\rho = c_A + c_B, \tag{23a}$$

$$\eta = k_A c_A - k_B c_B, \tag{23b}$$

so that the following decoupled problems result

$$\frac{\partial \rho}{\partial t} = \mathscr{D}\nabla^2 \rho, \quad \text{in } \mathscr{V}_\beta, \tag{24a}$$

$$B.C. \; -\mathbf{n}\cdot\nabla\rho = 0, \quad \text{at } \mathscr{A}_{\beta\sigma}, \tag{24b}$$

$$\frac{\partial \eta}{\partial t} = \mathscr{D}\nabla^2 \eta, \quad \text{in } \mathscr{V}_\beta, \tag{25a}$$

$$B.C. \; -\mathbf{n}\cdot\nabla\eta = k_+\eta, \quad \text{at } \mathscr{A}_{\beta\sigma}. \tag{25b}$$

In the above equation, $k_+ = k_A + k_B$. This change of variables is quite convenient since Eq. (24) now correspond to the problem of passive diffusion in porous media, whereas Eq. (25) have the same mathematical structure as for coupled diffusion and first-order heterogeneous reaction studied in Sect. 2.1. Therefore, the corresponding upscaled model is composed of the following set of equations

$$\frac{\partial \langle\rho\rangle^\beta}{\partial t} = \nabla\cdot(\mathbf{D}_{eff}\cdot\nabla\langle\rho\rangle^\beta), \tag{26a}$$

$$\frac{\partial \langle\eta\rangle^\beta}{\partial t} = \nabla\cdot\left(\mathbf{D}_{effr}\cdot\nabla\langle\eta\rangle^\beta\right) - \frac{a_v k_{eff}}{\phi}\langle\eta\rangle^\beta. \tag{26b}$$

The effective medium coefficients, for which the nomenclature for VAM is used, are defined exactly in the same way as in the previous section. Therefore, on the basis of the definitions given in Eq. (23), the following macroscale model results

$$\phi\frac{\partial \langle c_A\rangle^\beta}{\partial t} = \nabla\cdot\left[\phi\left(\mathbf{D}^{aa}_{effr}\cdot\nabla\langle c_A\rangle^\beta + \mathbf{D}^{ab}_{effr}\cdot\nabla\langle c_B\rangle^\beta\right)\right] - \frac{a_v k_{eff}}{k_+}\left(k_A\langle c_A\rangle^\beta - k_B\langle c_B\rangle^\beta\right), \tag{27a}$$

$$\phi\frac{\partial \langle c_B\rangle^\beta}{\partial t} = \nabla\cdot\left[\phi\left(\mathbf{D}^{bb}_{effr}\cdot\nabla\langle c_B\rangle^\beta + \mathbf{D}^{ba}_{effr}\cdot\nabla\langle c_A\rangle^\beta\right)\right] + \frac{a_v k_{eff}}{k_+}\left(k_A\langle c_A\rangle^\beta - k_B\langle c_B\rangle^\beta\right). \tag{27b}$$

In the above equations, the apparent main diffusion and co-diffusion coefficients are defined according to Eqs. (27) and (28) in [21] with $\mathbf{D}^{\gamma\kappa}_{effr} \equiv \mathbf{D}^{hom}_{\gamma\kappa}$ and $\mathbf{D}_{eff} \equiv \mathbf{D}^{hom}$, and can be expressed as follows ($\gamma, \kappa = a, b$, while, implicitly, a, b denote species A, B)

$$\mathbf{D}^{\gamma\kappa}_{effr} = \frac{1}{k_+}\left[\mathbf{D}_{effr}\,k_\kappa(-1)^{1-\delta^K_{\gamma\kappa}} + \mathbf{D}_{eff}\,k_A(\delta^K_{\gamma b} + \alpha\delta^K_{\gamma a})\right]. \tag{28}$$

Here $\delta^K_{\gamma\kappa}$ is the Kronecker delta and $\alpha = k_B/k_A$. This generic formula shows that, besides knowledge of the reaction rate coefficients for both species, only the values of $\mathbf{D}_{effr}$ and $\mathbf{D}_{eff}$ are required in order to predict the four apparent diffusion and co-diffusion coefficients. In other words, only two closure problems need to be solved in order to predict all the effective medium coefficients involved in this model, which is clearly an advantage with respect to the approach reported in [20], where it was proposed to solve four closure problems to predict the effective medium coefficients.

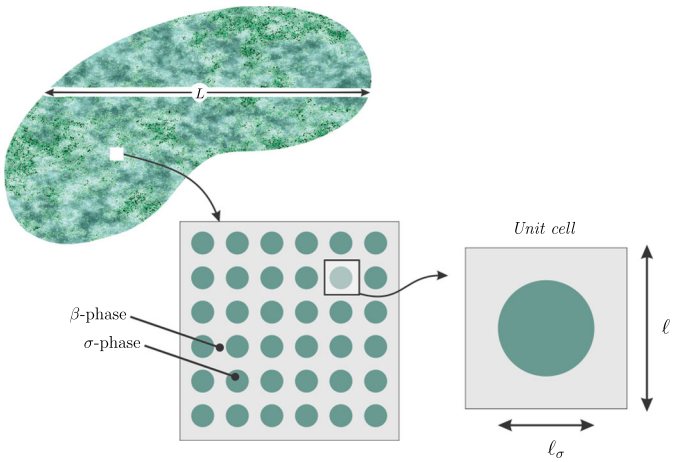

Fig. 2 Sketch of the periodic unit cell used to carry out the numerical solution of the closure problems

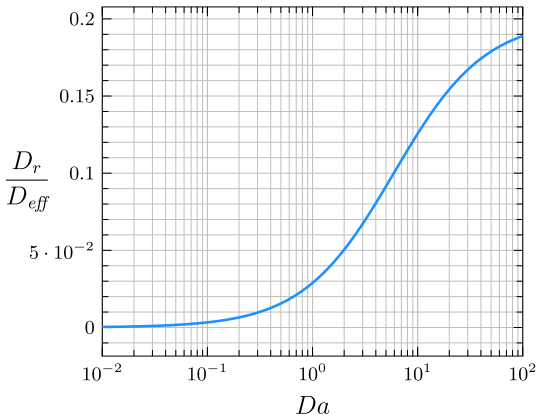

Fig. 3 Dependence of the reactive term in the apparent effective diffusivity on the Damköhler number (Da). The porosity value is 0.8

3 Results and discussion

The purpose of this section is to provide predictions of the effective medium coefficients involved in the upscaled models reported in the previous sections and to investigate their validity by comparison with pore-scale simulations. To this end, the attention is first directed to the case of diffusion and reaction involving a single chemical species, and subsequently, two chemical species. In both cases, the numerical solution of the closure problems is carried out modeling the porous medium microstructure as an array of inline cylinders of circular cross section as sketched in Fig. 2. This corresponds to the geometry considered in [21,24], and it has the convenient feature that the diffusivity tensors become spherical, so that it is only necessary to compute the single nonzero component of these tensors. In addition, the numerical results presented here correspond to a porosity value of 0.8.

All the numerical simulations reported in this work were performed using the finite-element software Comsol Multiphysics 6.2 employing the mass transfer modules, except for problems ψ and $\boldsymbol{\chi}_r$. For these two problems, the coefficient form PDE and the general form PDE modules available in the Comsol software were used, respectively, as recommended in [21]. In addition, standard meshing tests were performed in order to ensure that the results presented here are those obtained when mesh convergence is reached.

3.1 Diffusion and reaction involving one chemical species

In the case of only one species experiencing coupled diffusion and heterogeneous reaction, the interest lies first upon predicting the values of $\mathbf{D}_{eff_r}$ ($\mathbf{D}_r^{hom}$) and k_{eff} ($\mathcal{K}$) by solving the associated closure problems deduced

from the volume averaging method (VAM) and from the periodic homogenization method using the spectral approach (PHM). Commencing with the diffusion coefficient, in Fig. 3, the reactive part of the apparent diffusion coefficient, normalized by the intrinsic effective diffusion coefficient, D_r/D_{eff} (see Eq. (18)), is reported vs. the Damköhler number ($Da = k\ell/\mathscr{D}$, with ℓ being the side-length of the periodic unit cell (see Fig. 2)). As expected, this coefficient tends to zero for $Da \ll 1$ and increases with this dimensionless number until reaching values that can be more than 0.15 times the intrinsic effective diffusion coefficient. The fact that the purely reactive part of D_{effr} can be isolated is certainly an advantage that VAM offers, whereas the same is not possible to achieve with PHM. Indeed, this decomposition is possible in VAM due to the linear nature of the pore-scale model that is maintained in closure problems I and II. Unfortunately, the same is not true for problems ψ and $\boldsymbol{\chi}_r$ in the PHM with the spectral approach.

In Fig. 4a, the predictions of the effective reaction rate coefficients are reported as functions of the Damköhler number. Clearly, the predictions from VAM and PHM perfectly match for $Da \leq 1$. For larger values, results start to differ and can reach a relative difference up to about 14% for $Da = 100$. In the same figure, the results from PHM are shown to correspond to those reported in Fig. 5c in [21]. Note that in this reference, $\mathcal{K}_a^{III}/\mathcal{K}_a^{II} = \mathcal{K}_b^{III}/\mathcal{K}_b^{II} = \mathcal{K}/(ka_v)$. Furthermore, the predictions that these authors reported to correspond to VAM only match those of this work in the limit $Da \to 0$.

In Fig. 4b, the predictions of the apparent effective diffusion coefficient resulting from both PHM and VAM are reported normalized by the intrinsic effective diffusion coefficient. In this case, the PHM results follow an opposite trend compared to those from VAM, which is consistent with 5(a) in [21]. As already pointed out in Fig. 4a, the numerical solution of the spectral closure problems leads to values of D_r^{hom} that match those reported in [21]. On the contrary, noticeable differences appear between the predictions corresponding to VAM from the present work and those reported by Bourbatache et al. with the same approach. Unfortunately, in this reference it is not made clear how the results from VAM were obtained. It is thus of importance to clarify this point by reporting the correct VAM predictions.

At this point, neither the VAM or PHM approaches can be judged to be the correct one. Therefore, the final part of the analysis is dedicated to the validity of the models using pore-scale simulations (PSS) considering that the system has reached steady state. These simulations were performed following [21], i.e., solving the pore-scale equations (1) with no accumulation term in a horizontal array of N unit cells ($N = 20$ for all the simulations), imposing periodicity conditions at the top and bottom boundaries and Dirichlet-type boundary conditions at the left (i.e., $x = 0$) and right (i.e., $x = L = N\ell$) macroscopic boundaries. Under these conditions, the pore-scale problem used for PSS can be expressed as follows ($c \equiv c(x, y)$)

$$0 = \nabla \cdot (\mathscr{D}\nabla c), \quad \text{in } \mathscr{V}_\beta, \tag{29a}$$

$$B.C.1 \quad -\mathbf{n} \cdot \mathscr{D}\nabla c = kc, \quad \text{at } \mathscr{A}_{\beta\sigma}, \tag{29b}$$

$$B.C.2 \quad c(x, 0) = c(x, \ell), \tag{29c}$$

$$B.C.3 \quad c(0, y) = c_{in}, \quad \text{at } x = 0, \tag{29d}$$

$$B.C.4 \quad c(L, y) = c_{\text{out}}, \quad \text{at } x = N\ell. \tag{29e}$$

In the above equations, c_{in} and c_{out} are the concentration values at the macroscopic inlet and outlet boundaries that are assumed to be constant in the following. Since the VAM and PHM upscaled models have the same mathematical structure, they can be solved analytically to yield the following expression

$$\langle c^* \rangle^\beta = \frac{\sinh\left[\varphi\,(N - x^*)\right]}{\sinh\left(\varphi N\right)}. \tag{30}$$

Here, $\langle c^* \rangle^\beta \equiv (\langle c \rangle^\beta - c_{out})/(c_{in} - c_{out})$, $x^* \equiv x/\ell$, and,

$$\varphi = \sqrt{\frac{k_{eff} a_v^* Da\,\mathscr{D}}{k\phi D_{effr}}}\ \text{(VAM)}, \quad \text{or} \quad \varphi = \sqrt{\frac{\mathcal{K}\ell Da\,\mathscr{D}}{k D_r^{hom}}}\ \text{(PHM)}. \tag{31}$$

In Fig. 5a, the predictions of the dimensionless intrinsic average concentration profiles resulting from PSS are compared with those from VAM and PHM. Clearly, both upscaling approaches reproduce the PSS concentration profiles in a satisfactory manner. Nevertheless the predictions from PHM exhibit a more noticeable difference with PSS than those from VAM as the Damköhler number is increased. Similar observations are applicable for the predictions of the dimensionless macroscopic diffusive flux $\langle j^* \rangle^\beta \equiv \langle j \rangle^\beta \ell/(\mathscr{D}(c_{in} - c_{out}))$ as reported in Fig. 5b. In order to provide a more quantitative view of the results presented in Fig. 5a, the %

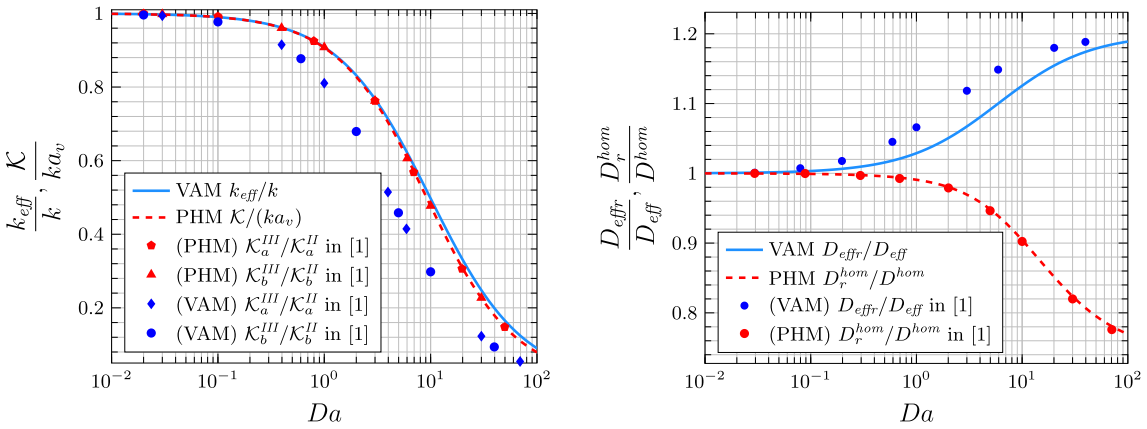

Fig. 4 Predictions of **a** the effective reaction rate coefficient and **b** the effective diffusivity versus the Damköhler number (Da) resulting from the volume averaging method (VAM) and the periodic homogenization method involving the spectral approach (PHM). In addition, the numerical results reported in [21] are included as symbols. In all the simulations, the porosity is $\phi = 0.8$

errors between the predictions of the average concentration from the VAM and PHM models and the results from PSS are reported in Fig. 6 for $Da = 0.01$, 0.1, 1 and 10, taking the PSS concentration values as the reference. It must be noted that this relative error reaches quite large values due to the fact that the average concentration is very small and decreases as x^* increases with even a larger rate as Da increases, the species being more rapidly consumed right after the entrance of the medium as the reaction rate increases. Moreover, as expected, it becomes more difficult for the upscaled models to reproduce the average concentration profiles obtained from PSS as Da increases, especially near the entrance of the system. This is because as Da increases, the average concentrations exhibit spatial variations over a length scale that becomes compatible with the microscale, and the length scale constraint is no longer rigorously valid. In all cases reported here, the error resulting from PHM is larger than the one obtained from VAM.

At this point, it is not yet clear if either the PHM model or the one derived with VAM provides the correct predictions of the apparent effective diffusion coefficient. To address this very important issue, the 1D steady-state version of Eq. (11) is integrated between two arbitrary points (x_1 and x_2) to obtain

$$D_{effr} = \frac{k_{eff} a_v}{\phi} \frac{\int_{x_1}^{x_2} \langle c \rangle^\beta \, dx}{\left. \frac{d\langle c \rangle^\beta}{dx} \right|_{x_1}^{x_2}}. \tag{32}$$

All the terms on the right-hand side of the above equation can be determined from PSS except k_{eff}, which can be considered as being obtained from the closure problem solution corresponding either to VAM (Problem II given in Eq. (8)) or PHM (Problem ψ given in Eq. (20)). Therefore, in the following, the predictions of D_{effr} with k_{eff} resulting from VAM are referred to as PSS(VAM) and those using the reaction coefficient from PHM are denoted by PSS(PHM). Using the above equation (taking $x_1 = \ell/2$ and $x_2 = L - \ell/2$), the results reported in Fig. 7 are obtained. Clearly, the apparent effective diffusivity computed from VAM reproduces correctly the results from PSS(VAM), which confirm that the correct trend is for this coefficient to increase with the Damköhler number. In addition, the PSS(PHM) results only coincide with those from both VAM and PSS(VAM) for sufficiently small values of the Damköhler number (i.e., $Da < 0.1$). This shows that PHM using the spectral approach is inadequate to predict the apparent effective diffusion coefficient.

To further investigate the source of differences between PHM using the spectral approach and VAM, in Appendix D the upscaling process using the spectral approach is carried out employing the volume averaging method. Interestingly, the analysis shows that the same upscaled model and ancillary problems deduced from PHM are retrieved using VAM. This means that the source of discrepancy in the predictions of the effective medium coefficients is the change of variables involved in the spectral approach and not the upscaling process. This remark is relevant and explains why in this particular problem, differences arise between VAM and PHM, whereas in many other studies dealing with transport phenomena in multiscale systems, both approaches yield the exact same upscaled models and closure problems.

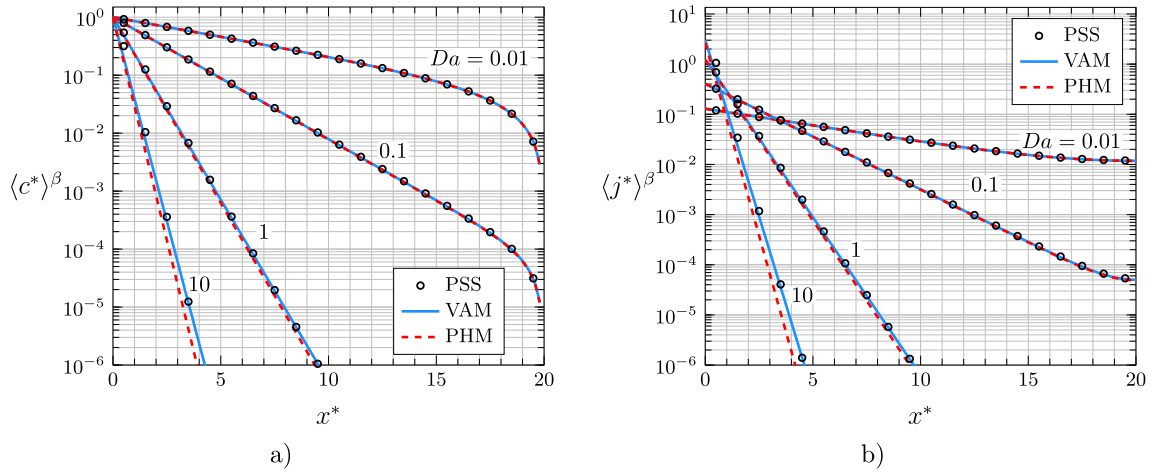

Fig. 5 Comparison of the predictions of the profiles of **a** the intrinsic average concentration, **b** the intrinsic average of the mass flux obtained using pore-scale simulations (PSS), the volume averaging method (VAM) and the periodic homogenization method (PHM) using the spectral approach reported in [21]. The continuous and dashed lines, respectively, result from the analytical solution (see Eq. (30)) of the VAM and PHM models. The porosity is taken to be $\phi = 0.8$

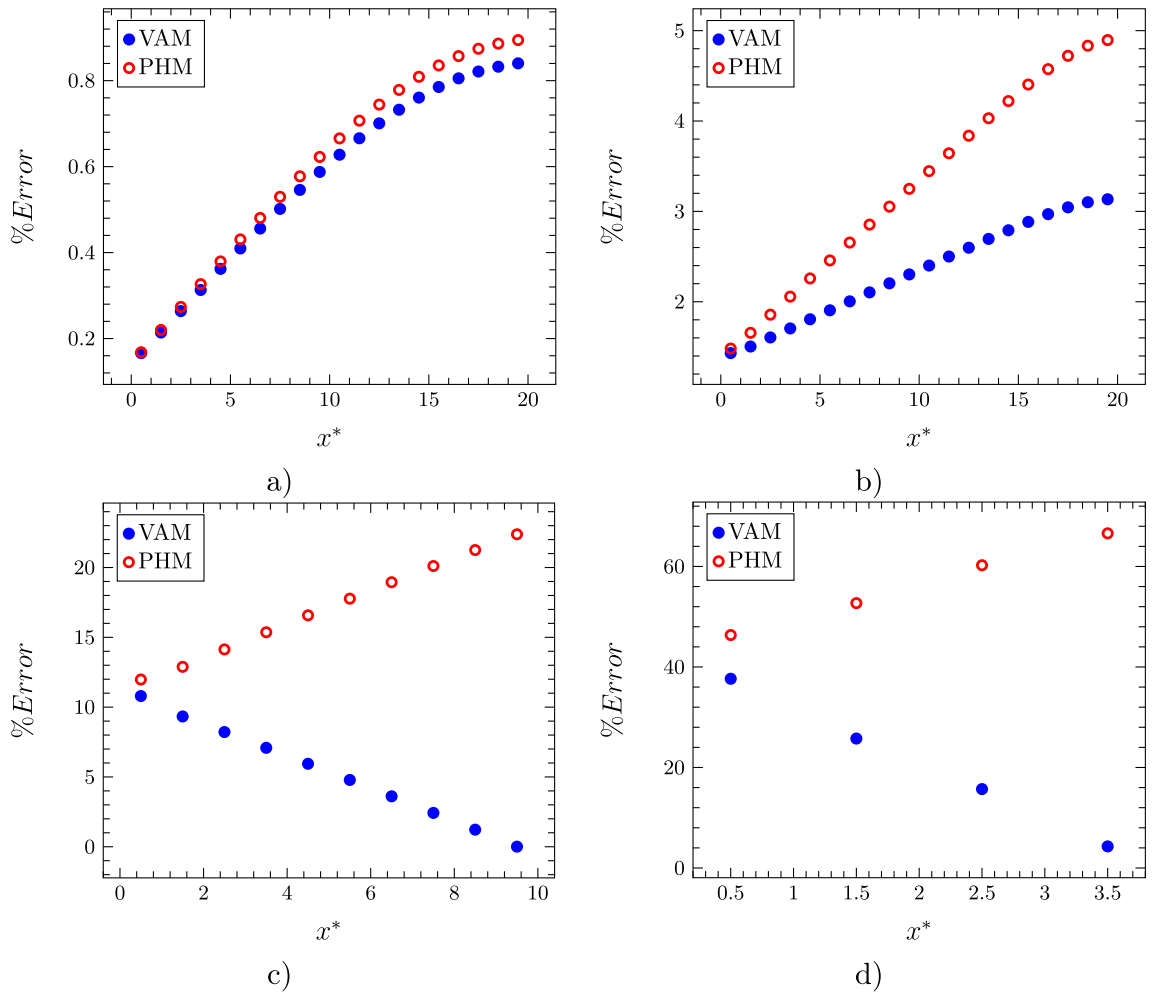

Fig. 6 Percent error between the upscaled models (VAM and PHM) relative to PSS corresponding to the predictions of the concentration profiles reported in Fig. 5a). The results correspond to **a** $Da = 0.01$, **b** $Da = 0.1$, **c** $Da = 1$ and **d** $Da = 10$

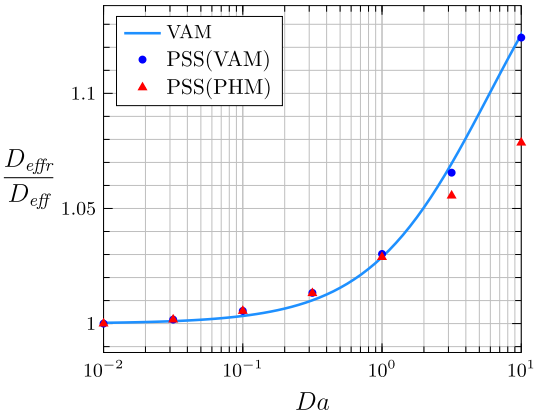

Fig. 7 Predictions of the apparent effective diffusivity D_{effr}, normalized by the effective diffusivity in the absence of reaction, D_{effr}, from the volume averaging method (VAM) compared to those obtained from pore-scale simulations, taking the effective reaction coefficient resulting from VAM (PSS(VAM)) and from PHM (PSS(PHM)). The porosity value is 0.8

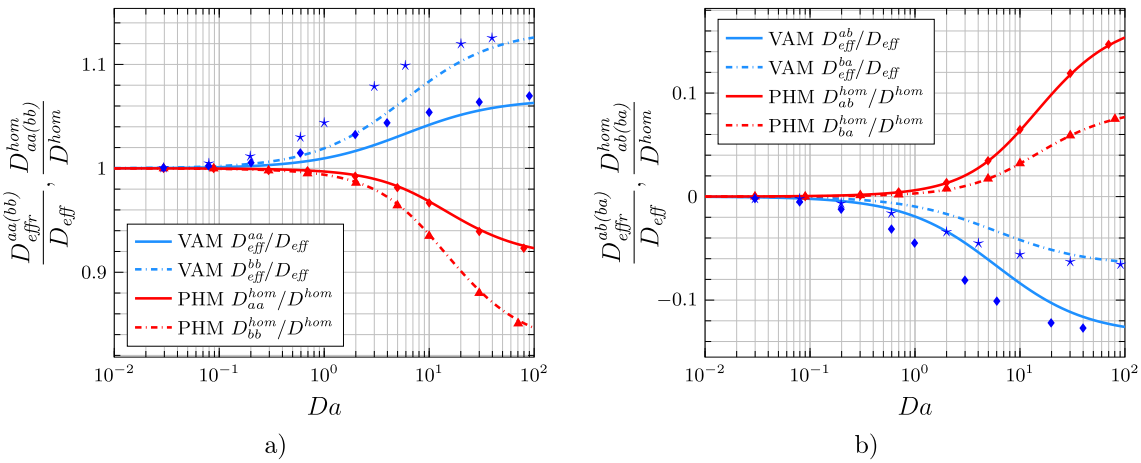

Fig. 8 Predictions of the main and co-diffusion coefficients resulting from the volume averaging method (VAM) and the periodic homogenization method (PHM) versus Da. In addition, the numerical results reported in [21] are included as the following symbols: in **a** ♦ (PHM) D^{hom}_{aa}/D^{hom}, ▲ (PHM) D^{hom}_{bb}/D^{hom}, ♦ (VAM) D^{aa}_{effr}/D_{eff}, ⋆ (VAM) D^{bb}_{effr}/D_{eff}; in **b** ♦ (PHM) D^{hom}_{ab}/D^{hom}, ▲ (PHM) D^{hom}_{ba}/D^{hom}, ♦ (VAM) D^{ab}_{effr}/D_{eff}, ⋆ (VAM) D^{ba}_{effr}/D_{eff}. In all the simulations the porosity is 0.8 and $\alpha = 2$

3.2 Diffusion and reaction involving two chemical species

To conclude this section, it is convenient to redirect the attention to the case of diffusive mass transport with two chemical species. As explained in the previous sections, the predictions of the effective medium coefficients in this case are straightforwardly obtained from their counterparts containing a single species [21] (see Eq. (28)). This means that the analysis and validation process presented above can be readily extended to this situation. The only remaining point to be clarified are the VAM predictions reported in 5 of ref. [21]. This issue is addressed in Fig. 8, where it is shown that the VAM predictions reported by Bourbatache et al. do not correspond to those from VAM of the present work. In contrast, the PHM results in the present study perfectly coincide with those reported in 5 in [21].

4 Conclusion

In this work, the upscaled model for coupled diffusion and heterogeneous reaction in homogeneous porous media is revisited, focusing on the regime where the reaction characteristic time is shorter than the one for diffusion, a situation characterized by a Damkhöler number, Da, larger than unity. Triggered by the differences raised by Bourbatache et al. [21] between the average model obtained from the volume averaging method

(VAM) on the one hand and that obtained from the periodic homogenization method (PHM) on the other hand, the present work brings two major clarifications, in addition to providing correct values of the effective coefficients involved in the model obtained from VAM, which were incorrectly reported in Bourbatache et al.

First, the controversy raised in Bourbatache et al. regarding the dependency of the apparent effective diffusion coefficient upon Da is alleviated. Indeed, the apparent effective diffusion coefficient involved in the model reported in [21,24] decreases with Da, whereas the one in the VAM model increases. A conclusive settlement regarding this controversy is reached by computing the apparent effective diffusion coefficient from direct pore-scale simulations treated as in silico experiments for Da up to 10. The results obtained from these numerical experiments are shown to be in very good agreement with the prediction of this coefficient from the closure problem derived with VAM. The physical interpretation of the increasing dependence of this coefficient on Da lies in the fact that the corrective contribution from reaction is positive and grows with Da.

Second, from direct pore-scale simulations, it is shown that the model obtained with VAM outperforms the predictions of the average concentration and flux with respect to the PHM model used in [21]. This motivates investigating alternative PHM upscaling derivations that are compatible with VAM and prone to reproduce PSS not only in terms of the average concentration and its gradient, but also in terms of the apparent effective diffusion coefficient. Finally, the analysis performed in this work (as shown in Appendix D) evidences that the source of discrepancy in the predictions of the effective medium coefficients does not lie in the upscaling process but in the change of variables proposed in the spectral approach.

Acknowledgements Authors warmly thank C. Geindreau from Univ. Grenoble-Alpes (France) for insightful discussions regarding this work. The analysis reported here was made possible thanks to the winter school APPRISE (Fundamentals of trAnsport Phenomena in PoRous medIa across ScalEs) that was organized by the France InterPore Chapter during February 2024 in Aussois, France. Support from the CNRS and RRI BEST-Usine du Futur of the University of Bordeaux is gratefully acknowledged by both authors. Data reported in this manuscript are all available upon request to the authors.

Funding No funding was received for conducting this study.

Declarations

Conflict of interest The authors have no relevant financial or non-financial interests to disclose.

Appendix A Derivation of the upscaled model using the adjoint and Green's formulation method

The objective of this appendix is to determine expressions for the two integral terms containing the concentration deviations in Eq. (4). To this end, let the derivations begin by considering the following Green's formula to relate the fields of a scalar a and a vector $\mathbf{a}$, both having the required regularity

$$\int_{\mathscr{V}_\beta} \left(a\nabla^2\mathbf{a} - \nabla^2 a\,\mathbf{a}\right)\, dV = \int_{\mathscr{A}_\beta} \mathbf{n}\cdot\left(a\nabla\mathbf{a} - \nabla a\,\mathbf{a}\right)\, dA, \tag{A1}$$

in which $\mathscr{A}_\beta$ represents the surface enclosing $\mathscr{V}_\beta$ that can be decomposed into the entrance and exit surfaces, $\mathscr{A}_{\beta e}$ and the interface with the σ phase, $\mathscr{A}_{\beta\sigma}$. Identifying a as $\mathscr{D}\tilde{c}$ and $\mathbf{a}$ as $\mathbf{d}$ in the above equation yields

$$\int_{\mathscr{V}_\beta} \left(\tilde{c}\mathscr{D}\nabla^2\mathbf{d} - \mathscr{D}\nabla^2\tilde{c}\,\mathbf{d}\right)\, dV = \int_{\mathscr{A}_\beta} \mathbf{n}\cdot\left(\tilde{c}\mathscr{D}\nabla\mathbf{d} - \mathscr{D}\nabla\tilde{c}\,\mathbf{d}\right)\, dA. \tag{A2}$$

Here, $\mathbf{d}$ is a vector that is to be defined from a boundary value (adjoint) problem, which is constructed in what follows. After substitution of the information contained in the boundary value problem defined in Eq. (5), this

leads to

$$\int_{\mathscr{V}_\beta}\left[\tilde{c}\mathscr{D}\nabla^2\mathbf{d}+\left(\frac{ka_v}{\phi}\langle c\rangle^\beta+\frac{k}{V_\beta}\int_{\mathscr{A}_{\beta\sigma}}\tilde{c}\,dA\right)\mathbf{d}\right]dV=\int_{\mathscr{A}_{\beta e}}\mathbf{n}\cdot(\tilde{c}\mathscr{D}\nabla\mathbf{d}-\mathscr{D}\nabla\tilde{c}\,\mathbf{d})\,dA$$
$$+\int_{\mathscr{A}_{\beta\sigma}}\left[\mathbf{n}\cdot(\tilde{c}\mathscr{D}\nabla\mathbf{d})+\left(\mathbf{n}\cdot\mathscr{D}\nabla\langle c\rangle^\beta+k\langle c\rangle^\beta+k\tilde{c}\right)\mathbf{d}\right]dA. \tag{A3}$$

To simplify this equation, the following boundary conditions and average constraint are proposed for $\mathbf{d}$

$$B.C.\quad -\mathbf{n}\cdot\mathscr{D}\nabla\mathbf{d}-k\mathbf{d}=\mathscr{D}\mathbf{n},\quad \text{at } \mathscr{A}_{\beta\sigma}, \tag{A4a}$$
$$\mathbf{d}(\mathbf{r})=\mathbf{d}(\mathbf{r}+\mathbf{l}_i),\quad i=1,2,3, \tag{A4b}$$
$$\langle\mathbf{d}\rangle^\beta=\mathbf{0}. \tag{A4c}$$

Therefore, Eq. (A3) reduces to

$$\int_{\mathscr{V}_\beta}\tilde{c}\mathscr{D}\nabla^2\mathbf{d}\,dV=\int_{\mathscr{A}_{\beta\sigma}}\left[-\mathbf{n}\mathscr{D}\tilde{c}+\left(\mathbf{n}\cdot\mathscr{D}\nabla\langle c\rangle^\beta+k\langle c\rangle^\beta\right)\mathbf{d}\right]dA. \tag{A5}$$

At this point, it is pertinent to integrate Eq. (A4a) over $\mathscr{A}_{\beta\sigma}$. Taking into account the periodicity and spatial homogeneity conditions, and using the divergence theorem, the following compatibility condition is derived

$$\int_{\mathscr{V}_\beta}\mathscr{D}\nabla^2\mathbf{d}\,dV=-k\int_{\mathscr{A}_{\beta\sigma}}\mathbf{d}\,dA. \tag{A6}$$

In order to meet this condition, the following differential equation is proposed

$$\mathscr{D}\nabla^2\mathbf{d}=-\frac{k}{V_\beta}\int_{\mathscr{A}_{\beta\sigma}}\mathbf{d}\,dA,\quad \text{in } \mathscr{V}_\beta. \tag{A7}$$

With this equation, the closure problem given in Eq. (7) in the main text is recovered. In addition, substitution of the above result into Eq. (A5) yields, after few algebraic steps,

$$\frac{\mathscr{D}}{V_\beta}\int_{\mathscr{A}_{\beta\sigma}}\mathbf{n}\tilde{c}\,dA=\frac{\mathscr{D}}{V_\beta}\int_{\mathscr{A}_{\beta\sigma}}(\mathbf{nd})^T\,dA\cdot\nabla\langle c\rangle^\beta+\frac{1}{V_\beta}\int_{\mathscr{A}_{\beta\sigma}}k\mathbf{d}\,dA\,\langle c\rangle^\beta. \tag{A8}$$

Taking the divergence on both sides of the above equation, recalling the spatial invariance of the integral terms, leads to

$$\nabla\cdot\left(\frac{\mathscr{D}}{V_\beta}\int_{\mathscr{A}_{\beta\sigma}}\mathbf{n}\tilde{c}\,dA\right)=\frac{\mathscr{D}}{V_\beta}\int_{\mathscr{A}_{\beta\sigma}}(\mathbf{nd})^T\,dA:\nabla\nabla\langle c\rangle^\beta+\frac{k}{V_\beta}\int_{\mathscr{A}_{\beta\sigma}}\mathbf{d}\,dA\cdot\nabla\langle c\rangle^\beta. \tag{A9}$$

Moving on to the second integral term in Eq. (4), consider now the following Green's formula for two scalar regular enough fields a and b

$$\int_{\mathscr{V}_\beta}\left(a\nabla^2b-\nabla^2a\,b\right)dV=\int_{\mathscr{A}_\beta}\mathbf{n}\cdot(a\nabla b-\nabla a\,b)\,dA. \tag{A10}$$

Taking $a=\mathscr{D}\tilde{c}$ and $b=s-1$, it follows that

$$\int_{\mathscr{V}_\beta}\left(\tilde{c}\mathscr{D}\nabla^2s-\mathscr{D}\nabla^2\tilde{c}\,(s-1)\right)dV=\int_{\mathscr{A}_\beta}\mathbf{n}\cdot(\tilde{c}\mathscr{D}\nabla s-\mathscr{D}\nabla\tilde{c}\,(s-1))\,dA. \tag{A11}$$

Here, again, s is a scalar that needs to be defined from a boundary value (or second adjoint) problem that is the purpose of the development that follows. After substitution of the differential equation and boundary conditions from Eq. (5), the above equation takes the form

$$\int_{\mathscr{V}_\beta} \left[\tilde{c}\mathscr{D}\nabla^2 s + \left(\frac{k a_v}{\phi} \langle c \rangle^\beta + \frac{k}{V_\beta} \int_{\mathscr{A}_{\beta\sigma}} \tilde{c}\, dA \right) (s-1) \right] dV$$
$$= \int_{\mathscr{A}_{\beta\sigma}} \left[\mathbf{n} \cdot \tilde{c}\mathscr{D}\nabla s + \left(\mathbf{n} \cdot \mathscr{D}\nabla \langle c \rangle^\beta + k\langle c \rangle^\beta + k\tilde{c} \right) (s-1) \right] dA$$
$$+ \int_{\mathscr{A}_{\beta e}} \mathbf{n} \cdot (\tilde{c}\mathscr{D}\nabla s - \mathscr{D}\nabla\tilde{c}\,(s-1))\, dA. \tag{A12}$$

From this equation, it is pertinent to propose the following boundary conditions and average constraint

$$B.C. \quad -\mathbf{n} \cdot \mathscr{D}\nabla s = ks, \quad \text{at } \mathscr{A}_{\beta\sigma}, \tag{A13a}$$
$$s(\mathbf{r}) = s(\mathbf{r} + \mathbf{l}_i), \quad i = 1, 2, 3, \tag{A13b}$$
$$\langle s \rangle^\beta = 1. \tag{A13c}$$

Consequently, Eq. (A12) reduces to

$$\int_{\mathscr{V}_\beta} \tilde{c}\mathscr{D}\nabla^2 s\, dV = \int_{\mathscr{A}_{\beta\sigma}} \left[-k\tilde{c} + \left(\mathbf{n} \cdot \mathscr{D}\nabla \langle c \rangle^\beta + k\langle c \rangle^\beta \right) (s-1) \right] dA. \tag{A14}$$

Furthermore, integration of Eq. (A13a) over $\mathscr{A}_{\beta\sigma}$ gives rise, after use of the divergence theorem, to the following compatibility condition

$$\int_{\mathscr{V}_\beta} \mathscr{D}\nabla^2 s\, dV = -k \int_{\mathscr{A}_{\beta\sigma}} s\, dA. \tag{A15}$$

As done before, in order to meet this condition, the following differential equation is proposed

$$\mathscr{D}\nabla^2 s = -\frac{k}{V_\beta} \int_{\mathscr{A}_{\beta\sigma}} s\, dA, \quad \text{in } \mathscr{V}_\beta. \tag{A16}$$

Note that by making the change of variable given in Eq. (8d), Eqs. (8a)–(8c) in the main text are retrieved. Substitution of the above expression into Eq. (A14) leads to

$$\frac{k}{V_\beta} \int_{\mathscr{A}_{\beta\sigma}} \tilde{c}\, dA = \frac{1}{V_\beta} \int_{\mathscr{A}_{\beta\sigma}} \mathscr{D} s \mathbf{n}\, dA \cdot \nabla \langle c \rangle^\beta + \frac{k}{V_\beta} \int_{\mathscr{A}_{\beta\sigma}} (s-1)\, dA \langle c \rangle^\beta. \tag{A17}$$

Here, the assumption of spatial homogeneity was used. Note that the above result can be further developed by recalling that $s = f/\langle f \rangle^\beta$ and using the result given in Eq. (B4) to obtain

$$\frac{k}{V_\beta} \int_{\mathscr{A}_{\beta\sigma}} \tilde{c}\, dA = \frac{k}{V_\beta} \int_{\mathscr{A}_{\beta\sigma}} \mathbf{d}\, dA \cdot \nabla \langle c \rangle^\beta + \frac{k}{V_\beta} \int_{\mathscr{A}_{\beta\sigma}} (s-1)\, dA \langle c \rangle^\beta. \tag{A18}$$

Substitution of this result and Eq. (A9) into Eq. (4) gives rise to the closed model obtained from VAM, written in Eq. (9) in the main text.

Appendix B Relationship between the closure variables d and f

In Sect. 2.1.1, the macroscopic model that follows from the introduction of the formal solution given in Eq. (6) into Eq. (4) yields macroscopic mass balance Eq. (9) that involves a convective-like term with an effective convective velocity $\mathbf{u}$ given by Eq. (10c). In this appendix, a formal relationship between the closure variables $\mathbf{d}$ and f is derived in order to formally show that $\mathbf{u} = 0$.
The proof starts by considering a Green's formula, given by

$$\int_{\mathscr{V}_\beta} \left(a\nabla^2\mathbf{a} - \nabla^2 a\,\mathbf{a}\right)\, dV = \int_{\mathscr{A}_\beta} \mathbf{n}\cdot\left(a\nabla\mathbf{a} - \nabla a\,\mathbf{a}\right)\, dA, \tag{B1}$$

in which, a and $\mathbf{a}$ are, respectively, arbitrary scalar and vector fields, having sufficient regularity, whereas $\mathscr{A}_\beta$ represents the surface enclosing $\mathscr{V}_\beta$ and $\mathbf{n}$ its unit normal vector pointing out of $\mathscr{V}_\beta$.
Taking $a = f$ and $\mathbf{a} = \mathbf{d}$ in this formula, recalling periodicity for both closure variables, and making use of Eqs. (7a), (7b), (8a) and (8b), yields

$$\int_{\mathscr{V}_\beta} \left(-\frac{k}{\mathscr{D}V_\beta} f \int_{\mathscr{A}_{\beta\sigma}} d\,dA + \frac{k}{\mathscr{D}} d\right)\, dV = -\int_{\mathscr{A}_{\beta\sigma}} nf\, dA. \tag{B2}$$

This equation can be equivalently written as

$$\frac{k}{\mathscr{D}}\left(-\langle f\rangle^\beta \int_{\mathscr{A}_{\beta\sigma}} \mathbf{d}\, dA + \int_{\mathscr{V}_\beta} \mathbf{d}\, dV\right) = -\int_{\mathscr{A}_{\beta\sigma}} \mathbf{n} f\, dA. \tag{B3}$$

Making further use of the average constraint on $\mathbf{d}$ expressed in Eq. (7d), this finally leads to

$$\frac{k}{\mathscr{D}}\langle f\rangle^\beta \int_{\mathscr{A}_{\beta\sigma}} d\, dA = \int_{\mathscr{A}_{\beta\sigma}} nf\, dA, \tag{B4}$$

which, after multiplying by $\frac{\mathscr{D}}{V_\beta\langle f\rangle^\beta}$ and from the definition of $\mathbf{u}$ given in Eq. (10c), proves that $\mathbf{u} = 0$.

Appendix C Symmetry and positiveness of $\mathbf{D}_{effr}$ (and $\boldsymbol{D}_{eff}$)

The proof of symmetry and positiveness of $\mathbf{D}_{effr}$ can be carried out by making use of the following Green's formula which holds for any second-order tensor $\boldsymbol{A}$ and vector $\mathbf{a}$ having sufficient regularity

$$\int_{\mathscr{V}_\beta} \left(\nabla\cdot\mathbf{A}\mathbf{a} + \mathbf{A}^T\cdot\nabla\mathbf{a}\right)\, dV = \int_{\mathscr{A}_\beta} \mathbf{n}\cdot\mathbf{A}\mathbf{a}\, dA. \tag{C1}$$

Here, $\mathscr{A}_\beta$ denotes the surface enclosing the domain $\mathscr{V}_\beta$ and $\mathbf{n}$ the unit normal vector at $\mathscr{A}_\beta$ pointing out of $\mathscr{V}_\beta$.
Taking $\mathsf{A} = \nabla\mathbf{d} + \mathsf{I}$ and $\mathbf{a} = \mathbf{d}$ in this formula and recalling periodicity, leads to

$$\int_{\mathscr{V}_\beta} \left(\nabla^2\mathbf{d}\,\mathbf{d} + \left(\nabla\mathbf{d}^T + \mathsf{I}\right)\cdot\nabla\mathbf{d}\right)\, dV = \int_{\mathscr{A}_{\beta\sigma}} \mathbf{n}\cdot\left(\nabla\mathbf{d} + \mathsf{I}\right)\mathbf{d}\, dA. \tag{C2}$$

Making use of Eqs. (7a),(7b) and (7d) in the above, and dividing the resulting equation by V_β, gives

$$\mathbf{0} = \langle\nabla\mathbf{d}^T\cdot\nabla\mathbf{d}\rangle^\beta + \langle\nabla\mathbf{d}\rangle^\beta + \frac{k}{\mathscr{D}V_\beta}\int_{\mathscr{A}_{\beta\sigma}} \mathbf{d}\mathbf{d}\, dA. \tag{C3}$$

At this point, it is convenient to recall the expression of $\mathbf{D}_{effr}$ given by $\mathbf{D}_{effr}/\mathscr{D} = \mathbf{I} + \langle \nabla \mathbf{d} \rangle^{\beta}$ and add it to the transpose of Eq. (C3), which yields

$$\frac{\mathbf{D}_{effr}}{\mathscr{D}} = \mathbf{I} + \langle \nabla \mathbf{d} \rangle^{\beta} + \langle \nabla \mathbf{d}^T \cdot \nabla \mathbf{d} \rangle^{\beta} + \langle \nabla \mathbf{d}^T \rangle^{\beta} + \frac{k}{\mathscr{D} V_{\beta}} \int_{\mathscr{A}_{\beta\sigma}} \mathbf{d}\mathbf{d}\, dA, \tag{C4}$$

or, equivalently,

$$\frac{\mathbf{D}_{effr}}{\mathscr{D}} = \left\langle (\nabla \mathbf{d} + \mathbf{I})^T \cdot (\nabla \mathbf{d} + \mathbf{I}) \right\rangle^{\beta} + \frac{k}{\mathscr{D} V_{\beta}} \int_{\mathscr{A}_{\beta\sigma}} \mathbf{d}\mathbf{d}\, dA. \tag{C5}$$

This expression proves that $\boldsymbol{D}_{\text{effr}}$ is a symmetric and positive tensor. Indeed, for any arbitrary constant vector $\boldsymbol{\lambda}$, $\boldsymbol{\lambda} \cdot \frac{\mathbf{D}_{effr}}{\mathscr{D}} \cdot \boldsymbol{\lambda} = \left\langle ((\nabla \mathbf{d} + \mathbf{I}) \cdot \boldsymbol{\lambda})^2 \right\rangle^{\beta} + \frac{k}{\mathscr{D} V_{\beta}} \int_{\mathscr{A}_{\beta\sigma}} (\boldsymbol{\lambda} \cdot \mathbf{d})^2\, dA \geq 0$. Moreover, in the absence of reaction, $k = 0$ and $\mathbf{d} \equiv \mathbf{b}$ leading to

$$\frac{\mathbf{D}_{eff}}{\mathscr{D}} = \left\langle (\nabla \mathbf{b} + \mathbf{I})^T \cdot (\nabla \mathbf{b} + \mathbf{I}) \right\rangle^{\beta}, \tag{C6}$$

which proves that $\mathbf{D}_{eff}$ is also a symmetric [27, sectionsIIC,IIIB] and positive tensor. Note that conclusions drawn from Eq. (C5) also hold in the regime $Da \leq 1$, since, in that case, the effective diffusion tensor is equal to $\mathbf{D}_{eff}$ [19].

Appendix D Application of VAM with the spectral approach

The purpose of this appendix is to analyze the spectral approach used in homogenization by employing the volume averaging method. In particular, it is of interest to determine if it is possible to retrieve the same upscaled model and closure problems derived with PHM using VAM. To meet this goal, following [24], the first step in the spectral approach is to propose the change of variables

$$c(\mathbf{x}, \mathbf{y}, t) = \exp(-\lambda t)\theta(\mathbf{x}, \mathbf{y}, t). \tag{D1}$$

Here, $\mathbf{x}$ and $\mathbf{y}$, respectively, represent the macroscale and microscale coordinates. In addition, λ is the first positive eigenvalue of an ancillary problem to be derived. The purpose of this change of variable is to allow diffusion and reaction to be of the same order of magnitude at the macroscale [22]. Substitution of equation (D1) into Eq. (1) leads to

$$\frac{\partial \theta}{\partial t} - \lambda\theta = \nabla \cdot (\mathscr{D} \nabla \theta), \quad \text{in } \mathscr{V}_{\beta}, \tag{D2a}$$

$$B.C. \quad -\mathbf{n} \cdot \mathscr{D} \nabla \theta = k\theta, \quad \text{at } \mathscr{A}_{\beta\sigma}. \tag{D2b}$$

This problem has a structure similar to that of unsteady diffusion of a chemical species undergoing both homogeneous and heterogeneous reactions in porous media. If the volume averaging method is applied to this problem, the resulting effective diffusion tensor would asymptotically tend to $\mathscr{D}\mathbf{I}$ at sufficiently large values of the Damköhler number as reported in the main text, which is opposite to the results reported in [21]. Therefore, the origin of the discrepancy is not lying on this first change of variable.
Following [24], the next step is to introduce a second change of variables,

$$\theta(\mathbf{x}, \mathbf{y}, t) = \psi(\mathbf{y}) v(\mathbf{x}, \mathbf{y}, t), \tag{D3}$$

in order to generate the following two ancillary problems

$$\nabla_{\mathbf{y}} \cdot (\mathscr{D} \nabla_{\mathbf{y}} \psi) = -\lambda\psi, \quad \text{in } \mathscr{V}_{\beta}, \tag{D4a}$$

$$B.C. \quad -\mathbf{n} \cdot \mathscr{D} \nabla_{\mathbf{y}} \psi = k\psi, \quad \text{at } \mathscr{A}_{\beta\sigma}, \tag{D4b}$$

$$\psi(\mathbf{r}) = \psi(\mathbf{r} + \mathbf{l}_i), \quad i = 1, 2, 3, \tag{D4c}$$

$$\langle \psi^2 \rangle^{\beta} = 1. \tag{D4d}$$

$$\psi^2 \frac{\partial v}{\partial t} = \nabla \cdot (\mathscr{D} \psi^2 \nabla v), \quad \text{in } \mathscr{V}_\beta, \tag{D5a}$$

$$B.C. \quad -\boldsymbol{n} \cdot \mathscr{D} \psi^2 \nabla v = 0, \quad \text{at } \mathscr{A}_{\beta\sigma} \tag{D5b}$$

It is important to note that, in the limit $k \to \infty$, Eq. (D4) indicated that $\psi \to 0$ at $\mathscr{A}_{\beta\sigma}$. Consequently, from Eq. (D5b), it results that ∇v is undefined at $\mathscr{A}_{\beta\sigma}$ in this limit, thus making it the problem defined by Eq. (D5) ill-posed.
The problem given in Eq. (D4) can be solved in a periodic unit cell, and ψ can thus be regarded as a known field of $\mathbf{y}$ in the following.
This allows focusing the attention on the problem defined in Eq. (D5). Application of the intrinsic averaging operator to Eq. (D5a), followed by the use of the spatial averaging theorem, taking into account the boundary condition given in Eq. (D5b) leads to

$$\left\langle \psi^2 \frac{\partial v}{\partial t} \right\rangle^\beta = \nabla \cdot \left\langle \mathscr{D} \psi^2 \nabla v \right\rangle^\beta. \tag{D6}$$

To make further progress, it is of interest to decompose v into its intrinsic average and spatial deviation in order to obtain the following expression

$$\frac{\partial \langle v \rangle^\beta}{\partial t} + \left\langle \psi^2 \frac{\partial \tilde{v}}{\partial t} \right\rangle^\beta = \nabla \cdot \left[\mathscr{D} \left(\nabla \langle v \rangle^\beta + \left\langle \psi^2 \nabla \tilde{v} \right\rangle^\beta \right) \right]. \tag{D7}$$

Note that the constraint given in Eq. (D4d) was used. The above equation is the unclosed model as it requires knowledge of $\tilde{v}$ in order to be complete. At this point, it is convenient to further develop the right-hand side of Eq. (D5a) to obtain

$$\psi^2 \frac{\partial v}{\partial t} = \psi^2 \nabla \cdot (\mathscr{D} \nabla v) + \cancel{\psi^{-2}} \nabla \psi^2 \cdot (\mathscr{D} \nabla v), \quad \text{in } \mathscr{V}_\beta. \tag{D8}$$

Subtracting Eq. (D7) (previously multiplied by ψ^2) to the above expression and using the spatial decomposition $v = \langle v \rangle^\beta + \tilde{v}$ leads to

$$\psi^2 \frac{\partial \tilde{v}}{\partial t} - \psi^2 \left\langle \psi^2 \frac{\partial \tilde{v}}{\partial t} \right\rangle^\beta = \psi^2 \nabla \cdot \left(\mathscr{D} \nabla \tilde{v} - \mathscr{D} \left\langle \psi^2 \nabla \tilde{v} \right\rangle^\beta \right) + \cancel{\psi^{-2}} \nabla \psi^2 \cdot (\mathscr{D} \nabla \tilde{v}) + \cancel{\psi^{-2}} \nabla \psi^2 \cdot (\mathscr{D} \nabla \langle v \rangle^\beta), \quad \text{in } \mathscr{V}_\beta. \tag{D9}$$

With the intention of simplifying the above expression, the following orders of magnitude estimates are proposed

$$\frac{\partial \tilde{v}}{\partial t} = \mathbf{O}\left(\left\langle \psi^2 \frac{\partial \tilde{v}}{\partial t} \right\rangle^\beta \right) = \mathbf{O}\left(\frac{\tilde{v}}{t_{ref}} \right), \tag{D10a}$$

$$\nabla \cdot (\mathscr{D} \nabla \tilde{v}) = \mathbf{O}\left(\frac{\mathscr{D} \tilde{v}}{\ell^2} \right). \tag{D10b}$$

Hence, on the basis of the constraint $\ell^2 / \mathscr{D} \ll t_{ref}$, the field of $\tilde{v}$ can be assumed to be quasi-steady. Furthermore, restricting the computation of $\tilde{v}$ to a periodic unit cell, with $\tilde{v}$ being periodic, it follows that $\left\langle \psi^2 \nabla \tilde{v} \right\rangle^\beta$ is spatially invariant. Under these conditions, Eq. (D9) reduces to

$$\nabla_{\mathbf{y}} \cdot (\mathscr{D} \psi^2 \nabla_{\mathbf{y}} \tilde{v}) = -\mathscr{D} \nabla_{\mathbf{y}} \psi^2 \cdot \nabla \langle v \rangle^\beta, \quad \text{in } \mathscr{V}_\beta. \tag{D11a}$$

The corresponding interfacial boundary condition results from substituting the spatial decomposition for v in Eq. (D5b).

$$B.C. \quad \mathbf{n} \cdot \mathscr{D} \psi^2 \nabla_{\mathbf{y}} \tilde{v} = -\mathbf{n} \cdot \mathscr{D} \psi^2 \nabla \langle v \rangle^\beta, \quad \text{at } \mathscr{A}_{\beta\sigma}. \tag{D11b}$$

The problem statement is completed with the periodicity condition

$$\tilde{v}(\mathbf{r}) = \tilde{v}(\mathbf{r} + \mathbf{l}_i),\ i = 1, 2, 3, \tag{D11c}$$

and the average constraint

$$\langle \tilde{v} \rangle^{\beta} = 0. \tag{D11d}$$

This problem is linear in $\tilde{v}$ and its formal solution can therefore be expressed in terms of the unique source $\nabla \langle v \rangle^{\beta}$ as follows

$$\tilde{v} = \boldsymbol{\chi}_r \cdot \nabla \langle v \rangle^{\beta}. \tag{D12}$$

The closure variable $\boldsymbol{\chi}_r$ solves the boundary value problem given in Eq. (21) in the main text.
Substitution of the above expression into Eq. (D7), recalling the quasi-steady assumption for $\tilde{v}$, leads to

$$\phi \frac{\partial \langle v \rangle^{\beta}}{\partial t} = \nabla \cdot \left(\mathsf{D}_r^{hom} \cdot \nabla \langle v \rangle^{\beta} \right). \tag{D13}$$

Here, $\mathsf{D}_r^{hom} = \phi \langle \mathscr{D} \psi^2 (\mathsf{I} + \nabla_{\mathbf{y}} \boldsymbol{\chi}_r) \rangle^{\beta}$ as stated in Eq. (19a) in the main text. Furthermore, the result of applying the intrinsic averaging operator in Eq. (D1), taking into account (D3), is

$$\langle c \rangle^{\beta} = \exp(-\lambda t)\, \langle \psi v \rangle^{\beta}, \tag{D14}$$

or, after spatially decomposing v, recalling the formal solution given in Eq. (D12),

$$\langle c \rangle^{\beta} = \exp(-\lambda t) \left(\langle \psi \rangle^{\beta} \langle v \rangle^{\beta} + \left\langle \psi \boldsymbol{\chi}_r \right\rangle^{\beta} \cdot \nabla \langle v \rangle^{\beta} \right). \tag{D15}$$

To simplify this expression, the following orders of magnitude estimates are proposed

$$\langle \psi \rangle^{\beta} \langle v \rangle^{\beta} = \mathbf{O}\left(\langle v \rangle^{\beta} \right), \tag{D16a}$$

$$\left\langle \psi \boldsymbol{\chi}_r \right\rangle^{\beta} \cdot \nabla \langle v \rangle^{\beta} = \mathbf{O}\left(\frac{\ell}{L} \langle v \rangle^{\beta} \right). \tag{D16b}$$

On the basis of the length scale constraint $\ell \ll L$, it is reasonable to assume that

$$\left\langle \psi \boldsymbol{\chi}_r \right\rangle^{\beta} \cdot \nabla \langle v \rangle^{\beta} \ll \langle \psi \rangle^{\beta} \langle v \rangle^{\beta}. \tag{D17}$$

Consequently, Eq. (D15) reduces to

$$\langle c \rangle^{\beta} = \exp(-\lambda t)\, \langle \psi \rangle^{\beta} \langle v \rangle^{\beta}. \tag{D18}$$

With this result, Eq. (D13) is written in terms of $\langle c \rangle^{\beta}$ as follows:

$$\phi \frac{\partial \langle c \rangle^{\beta}}{\partial t} = \nabla \cdot \left(\mathbf{D}_r^{\mathrm{hom}} \cdot \nabla \langle c \rangle^{\beta} \right) - \mathcal{K} \langle c \rangle^{\beta}. \tag{D19}$$

Here, $\mathcal{K} = \phi \lambda$, as indicated in Eq. (19b) in the main text.
The above equation corresponds to Eq. (22) in [24] obtained with PHM. This analysis shows that the upscaled model reported in [24], as well as its closure problems, can be obtained also with the method of volume averaging. The key difference between this derivation and the one presented in Sect. 2.1.1 in the main text is the use of the changes of variables given in Eqs. (D1) and (D3). In other words, it is not the upscaling approach that makes the difference between this work and the one reported in [24] and [21]; it is the changes of variables used in the spectral approach.

References

1. Whitaker, S.: The method of volume averaging: an application to diffusion and reaction in porous catalysts. Proc. Natl. Sci. Counc. Part A: Phys. Sci. Eng. **15**(6), 465–474 (1991)
2. Whitaker, S.: The method of volume averaging. Springer, Dordrecht (1999). https://doi.org/10.1007/978-94-017-3389-2
3. Cerro, R.L., Higgins, B.G., Whitaker, S.: Material balances for chemical reacting systems, 1st edn. CRC Press, Boca Raton (2022). https://doi.org/10.1201/9781003283751
4. Le, T.D., Lasseux, D., Nguyen, X.P., Vignoles, G.L., Mano, N., Kuhn, A.: Multi-scale modeling of diffusion and electrochemical reactions in porous micro-electrodes. Chem. Eng. Sci. **173**, 153–167 (2017). https://doi.org/10.1016/j.ces.2017.07.039
5. Le, T.D., Zhang, L., Vignoles, G.L., Mano, N., Kuhn, A., Lasseux, D.: Optimal thickness of a porous micro-electrode operating a single redox reaction. ChemElectroChem **6**, 173–180 (2019). https://doi.org/10.1002/celc.201800972
6. Le, T.D., Zhang, L., Kuhn, A., Mano, N., Vignoles, G.L., Lasseux, D.: Upscaled model for diffusion and serial reduction pathways in porous electrodes. J. Electroanal. Chem. **855**, 113325 (2019). https://doi.org/10.1016/j.jelechem.2019.113325
7. Le, T.D., Lasseux, D.: Current and optimal dimensions predictions for a porous micro-electrode. ChemElectroChem **7**, 3017–3027 (2020). https://doi.org/10.1002/celc.202000508
8. Le, T.D., Mano, N., Kuhn, A., Lasseux, D.: Multiscale modelling of diffusion and enzymatic reaction in porous electrodes in direct electron transfer mode. Chem. Eng. Sci. **248**, 117157 (2022). https://doi.org/10.1016/j.ces.2021.117157
9. Auriault, J.-L., Boutin, C., Geindreau, C.: Homogenization of coupled phenomena in heterogenous media. ISTE LTD, London (2009)
10. Gray, W.G., Gray, G.A.: Introduction to environmental modeling. Cambridge University Press, Cambridge (2017)
11. Bear, J.: Modeling phenomena of flow and transport in porous media. Springer, Switzerland (2018). https://doi.org/10.1007/978-3-319-72826-1
12. Zhang, T., Zhang, P., Law, C.K., Qi, F.: CVD in weakly rarefied rotating disk flows. Chem. Vap. Deposition **15**, 274–280 (2009)
13. Bailey, J.E.: Biochemical reaction engineering and biochemical reactors. Chem. Eng. Sci. **35**(9), 1854–1886 (1980). https://doi.org/10.1016/0009-2509(80)80134-5
14. Gray, W.G., Miller, C.T.: Introduction to the thermodynamically constrained averaging theory for porous medium systems. Springer, Switzerland (2014). https://doi.org/10.1007/978-3-319-04010-3
15. Wood, B.D., Radakovich, K., Golfier, F.: Effective reaction at a fluid-solid interface: applications to biotransformation in porous media. Adv. Water Resour. **30**(6–7), 1630–1647 (2007). https://doi.org/10.1016/j.advwatres.2006.05.032
16. Valdes-Parada, F.J., Alvarez-Ramirez, J.: On the effective diffusivity under chemical reaction in porous media. Chem. Eng. Sci. **65**(13), 4100–4104 (2010). https://doi.org/10.1016/j.ces.2010.03.040
17. Valdés-Parada, F.J., Aguilar-Madera, C.G., Álvarez-Ramírez, J.: On diffusion, dispersion and reaction in porous media. Chem. Eng. Sci. **66**(10), 2177–2190 (2011). https://doi.org/10.1016/j.ces.2011.02.016
18. Lugo-Méndez, H.D., Valdés-Parada, F.J., Porter, M.L., Wood, B.D., Ochoa-Tapia, J.A.: Upscaling diffusion and nonlinear reactive mass transport in homogeneous porous media. Transp. Porous Media **107**(3), 683–716 (2015). https://doi.org/10.1007/s11242-015-0462-4
19. Valdés-Parada, F.J., Lasseux, D., Whitaker, S.: Diffusion and heterogeneous reaction in porous media: the macroscale model revisited. Int. J. Chem. React. Eng. (2017). https://doi.org/10.1515/ijcre-2017-0151
20. Qiu, T., Wang, Q., Yang, C.: Upscaling multicomponent transport in porous media with a linear reversible heterogeneous reaction. Chem. Eng. Sci. **171**, 100–116 (2017). https://doi.org/10.1016/j.ces.2017.05.018
21. Bourbatache, M.K., Millet, O., Moyne, C.: Upscaling coupled heterogeneous diffusion reaction equations in porous media. Acta Mech. **234**, 2293–2314 (2023). https://doi.org/10.1007/s00707-023-03501-w
22. Mauri, R.: Dispersion, convection, and reaction in porous media. Phys. Fluids A **3**(5), 743–756 (1991). https://doi.org/10.1063/1.858007
23. Allaire, G., Raphael, A.-L.: Homogenization of a convection–diffusion model with reaction in a porous medium. C.R. Math. **344**(8), 523–528 (2007). https://doi.org/10.1016/j.crma.2007.03.008
24. Bourbatache, M.K., Millet, O., Moyne, C.: Upscaling diffusion-reaction in porous media. Acta Mech. **231**(5), 2011–2031 (2020). https://doi.org/10.1007/s00707-020-02631-9
25. Gray, W.G.: A derivation of the equations for multi-phase transport. Chem. Eng. Sci. **30**(2), 229–233 (1975). https://doi.org/10.1016/0009-2509(75)80010-8
26. Bottaro, A.: Flow over natural or engineered surfaces: an adjoint homogenization perspective. J. Fluid Mech. **877**, 1 (2019). https://doi.org/10.1017/jfm.2019.607
27. Lasseux, D., Valdés-Parada, F.J.: Symmetry properties of macroscopic transport coefficients in porous media. Phys. Fluids **29**(4), 043303 (2017). https://doi.org/10.1063/1.4979907

Publisher's Note Springer Nature remains neutral with regard to jurisdictional claims in published maps and institutional affiliations.

Springer Nature or its licensor (e.g. a society or other partner) holds exclusive rights to this article under a publishing agreement with the author(s) or other rightsholder(s); author self-archiving of the accepted manuscript version of this article is solely governed by the terms of such publishing agreement and applicable law.